Franklin Open 3 (2023) 100012

Contents lists available at ScienceDirect

Franklin Open

journal homepage: www.elsevier.com/locate/fraope

Event-triggering-based H_∞ load frequency control for multi-area cyber–physical power system under DoS attacks☆

Xingyue Liu [a,b], Kaibo Shi [a,d,e,*], Kun Zhou [b], Shiping Wen [c], Yiqian Tang [a], Lin Tang [a]

[a] School of Electronic Information and Electrical Engineering, Chengdu University, Chengdu, 610106, PR China
[b] Key Laboratory of Intelligent Manufacturing Quality Big Data Tracing and Analysis of Zhejiang Province, China Jiliang University, Hangzhou, 310018, PR China
[c] Australian AI Institute, Faculty of Engineering and Information Technology, University of Technology Sydney, Sydney, NSW 2007, Australia
[d] Engineering Research Center of Power Quality of Ministry of Education, Anhui University, Hefei 230601, PR China
[e] Institute of Electronic and Information Engineering of University of Electronic Science and Technology of China in Guangdong, 523808, PR China

ARTICLE INFO

Keywords:
Resilient H_∞ load frequency control scheme
Cyber–physical power system
Denial-of-service attacks
Adaptive event-triggering mechanism
Transmission interval-dependent loop functional approach

ABSTRACT

In this work, the event-triggering-based resilient H_∞ load frequency control (LFC) scheme under denial-of-service (DoS) attacks is developed for multi-area cyber–physical power system (MA-CPPS) with electric vehicles (EVs). In MA-CPPS, the sampled measurements are transmitted through the communication network, which may be subjected to the energy-limited DoS attack with a resilient index of maximum allowable continuous data losses. Meanwhile, a novel adaptive event-triggering mechanism (AETM) characterized by parameters disturbances and dynamic adjustment mechanism of triggering threshold can effectively reduce the occupation of network bandwidth and computational burden in practical operation of sampled-data LFC in MA-CPPS. Hence a sampled-data LFC model of considering energy-limited DoS attack and AETM is established firstly. Then based on a novel AETM transmission interval-dependent loop functional approach, a resilient H_∞ state-feedback controller is designed with guaranteed H_∞ performance and resilient index of energy-limited DoS attack. Finally, the effectiveness and superiority of our proposed scheme are verified by one-area and three-areas LFC CPPS.

1. Introduction

For more smoothly and safely operation of power system [1–4], load frequency control (LFC) system is applied to maintain system frequency and the exchange power between regions at the rated value by keeping the balance between power generation and electric load. The LFC control schemes have attracted lots of attractions. Considering deception attacks and a memory ETM, H_∞ LFC control scheme is investigated for a single-area power system by Ref. [5]. Considering the existence of electric vehicles (EVs) firstly, H_∞ LFC model for a single-area power system is developed in Ref. [6]. These results are developed based on the model of single area power system and without considering disturbance factors. Nevertheless, the modern power systems are interconnected with each other, resulting in larger sale. In the process of interconnecting of multi-area power system, the increasing disturbance factors are also need to be considered in the modeling of LFC power system.

Considering the interconnection of power system and the development of communication technologies, power systems are gradually developed as cyber–physical power systems (CPPSs) [7], where integrated with information control equipments, sensors and communication network. Owing to digital equipments come to replace continuous-time equipments in CPPSs nowadays, the sampled-data methods have been adopted in the LFC CPPSs control model. With regard to the sampled-data LFC schemes, one method is to implement it in sampled-data mode, while design it in continuous-time way [8–10]. However, these LFC control schemes are effective just in a small enough sampling period, which are not applicable to the signal transmission mechanism like ETM. The other way is to design sampled-data scheme of LFC system based on discrete theory, such as the digital PID controller

☆ This work was supported by the National Natural Science Foundation of China under Grant (No. 61703060, 12061088, 61802036 and 61873305), the Sichuan Science and Technology Program under Grant No. 21YYJC0469, the Project funded by China Postdoctoral Science Foundation under Grant Nos. 2020M683274 and 2021T140092, Supported by the Open Research Project of the State Key Laboratory of Industrial Control Technology, Zhejiang University, China (No. ICT2021B38), Guangdong Basic and Applied Basic Research Foundation (2021A1515011692), Engineering Research Center of Power Quality of Ministry of Education, Anhui University (No. KFKT202102), Open Research Fund Program of Data Recovery Key Laboratory of Sichuan Province (Grant No. DRN2103), supported by the Open Research Project of Key Laboratory of Intelligent Manufacturing Quality Big Data Tracing and Analysis of Zhejiang Province, China Jiliang University (Grant No. ZNZZSZ-CJLU2022-06).

* Corresponding author at: School of Electronic Information and Electrical Engineering, Chengdu University, Chengdu, 610106, PR China.
E-mail address: skbs111@163.com (K. Shi).

https://doi.org/10.1016/j.fraope.2023.100012
Received 4 January 2023; Accepted 19 February 2023
Available online 28 February 2023

design in LFC system [11], decentralized sliding mode LFC design with delay [12], event-triggering sliding mode LFC approach [13]. These methods [11–13] all treat the sampling period as a discrete step. But the discrete LFC system may be inapplicable to the practical operation of power system, for example, the sampling period in real operation is generally set in the range of [2 s, 4 s] under which the discrete period setting in [0.08 s, 0.3 s] cannot satisfy Shannon sampling principle in hydrothermal power system. For avoiding the above shortcomings, an input-delay method [14] is proposed to discuss the control design of sampled-data systems. Based on the input-delay method, a looped-functional approach is put forward in Ref. [15] and further developed in Ref. [16]. For given different PI controller gains, the stability of LFC system and a robust LFC design considering both sampling and transmission delays are proposed in Ref. [17]. Ref. [18] put forward a sampled-data and fast LFC scheme for multi-area power system with the penetration of wind power, but the load disturbances are not taken into consideration. Noting that various disturbance factors are ignored in these results, which motivates us to investigate a sampled-data LFC scheme for MA-CPPS based on input-delay method considering various disturbance factors.

In sampling-data LFC scheme, ETM is an effective scheme to achieve the purposes [19–23] of occupying less communication bandwidth resources and reducing the computation burden of control system, which is obviously better than stochastic and period sampling mechanism. Proper event triggering condition decides the performance of ETM designed. An adaptive event-triggering H_∞ LFC scheme for multi-area power systems is proposed by Ref. [4], where event-triggering threshold can be dynamically adjusted to save more limited network resources. An improved memory-based ETM takes recent sampled data and transmitted signals before into consideration to determine whether the newly sampled signal will be transmitted in Ref. [5]. A novel ETM with adaptive dynamic programming for LFC power system model is designed by Ref. [24]. Moreover, Ref. [25] proposes a dynamic triggered algorithm for multi-area nonlinear power system, which can effectively reduce the amount of transmitted packages. But the influence of parameters fluctuations in ETM and cyber attacks in communication network on triggering results are ignored in the above published works, which exist in actual operation of LFC system.

The application of open communication network in LFC power system will bring low cost and high flexibility, while is vulnerable to be attacked in actual operation. Attacks from the cyber layer may bring severe damages to control and monitoring system. Various kinds of attacks are studied in security control field, such as denial-of-service (DoS) attacks [26,27], reply attacks [28], and deception attacks [29–31]. The trustworthiness of transmitted data is comprised in deception attacks. DoS attacks can interrupt communication transmissions by injecting a large number of useless data to malicious occupy the limited network resources, which causes the losses of sampled data. Thus the main task of anti-network-attack control is to mitigate the influence of network attacks in the case of maintaining the stable state of power system. There are lots of existing results about the control scheme under network attacks. The behaviors of DoS attacks are assumed to be periodic in Ref. [32], and to satisfy Markov chain in Ref. [33]. For releasing the strong assumptions, Ref. [34] builds a general model by bounding frequency and duration of DoS attack. An aperiodic sampled-data scheme with the DoS duration bounds for designing resilient controller is proposed in Ref. [35]. However, the above results are obtained just in stochastic or period sampling mechanism, which is inferior to ETM in terms of communication bandwidth occupying rate and computation burden. As an improvement, event-triggering LFC schemes for MA-CPPS are developed under various cyber attack. Ref. [36] investigates a resilient event-triggered H_∞ LFC scheme for multi-area power systems with energy-limited DoS attacks. The problem of event-triggered H_∞ LFC for multi-area power system under hybrid cyber attacks, including DoS attack and deception attack has been developed by Ref. [37]. But the above two event-triggering LFC schemes under cyber attack are verified by simulation cases considering the sampling period less than 1s. It is not in line with actual requirements in real operation of LFC power system, owing to the fact of a typical sampling period being 1–3 s in the actual sampling LFC control system [3,18]. It promotes our efforts in designing the ETM scheme for the actual power system considering both parameters disturbances and cyber-attacks.

Motivated by the above analyses and observations, this paper investigates the event-triggered-based resilient H_∞ LFC scheme under DoS attacks for the MA-CPPS with EVs. The three main innovations are listed as follows:

(1) Firstly, taking nonlinear load disturbances into account, a continuous-time LFC model of MA-CPPS with EVs is established.

(2) Secondly, considering the stealth and energy limitation of DoS attacks in communication network, they are modeled as nonuniform sampling process with bounded interval. Combined with the above characteristics of DoS attack process, a novel AETM with parameters disturbances and dynamic adjustment mechanism of triggering threshold is proposed. Hence the sampling-data LFC model of MA-CPPS considering AETM and DoS attack is established.

(3) Thirdly, based on a novel AETM transmission interval-dependent loop functional approach, a resilient H_∞ state-feedback controller is designed with guaranteed H_∞ performance and resilient index of energy-limited DoS attack.

The main work we have done are summarizes as follows:

(1) The sampling-data LFC model of MA-CPPS based on input-delay method considering AETM, DoS attacks and load disturbances is established, by considering the DoS attack as nonuniform sampling process with bounded interval, a novel AETM with parameters disturbances and dynamic adjustment mechanism of triggering threshold, and load disturbances together.

(2) A novel AETM transmission interval-dependent loop functional approach is proposed to analyze the H_∞ performance and obtain the H_∞ controller scheme for the above established model. Thus Theorem 1 and Theorem 2 are obtained, which can acquire the control gains with the guaranteed H_∞ performance and resilient index of DoS attack.

(3) Case studies of one-area and three-areas CPPS are carried out to verify the effectiveness and superiority of our method. The impact of DoS attack on our proposed AETM is studied by one-area LFC CPPS and the guaranteed H_∞ performance with the resilient DoS attack of our designed PI controller is studied by three-areas CPPS.

The paper is organized as follows. The continuous-time LFC model of MA-CPPS with EVs and nonlinear disturbances, as well as the sampling-data LFC model of MA-CPPS based on input-delay method considering AETM and DoS attacks are given in Section 2. The H_∞ performance analysis method and resilient controller design are showed in Section 3. Case studies of one-area and three-areas CPPS are presented in Section 4. Section 5 concludes the whole work.

Notation: Let $\mathbb{R}$, $\mathbb{R}^n$, $\mathbb{R}^{n*m}$ denotes the set of real numbers, the n-dimensional Euclidean space, the set of all $n \times m$ real matrices, separately; P^{-1} and P^T denotes the inverse and transpose of a given matrix P; $P > 0$ stands for that the matrix P is real symmetric positive definite matrix; $col\{a_1, \dots, a_n\} = [a_1^T, \dots, a_n^T]^T$; $diag\{\dots\}$ represents a block-diagonal matrix; $sym\{X\} = X + X^T$; $\star$ in the matrix represents the symmetry of matrix.

2. Problem formulation

2.1. Continuous-Time LFC model of MA-CPPS with EVs and nonlinear disturbances

The LFC model of MA-CPPS with EVs is presented in Fig. 1. Where $e_k = 2\pi$. And the transfer functions listed in Fig. 1 are defined as

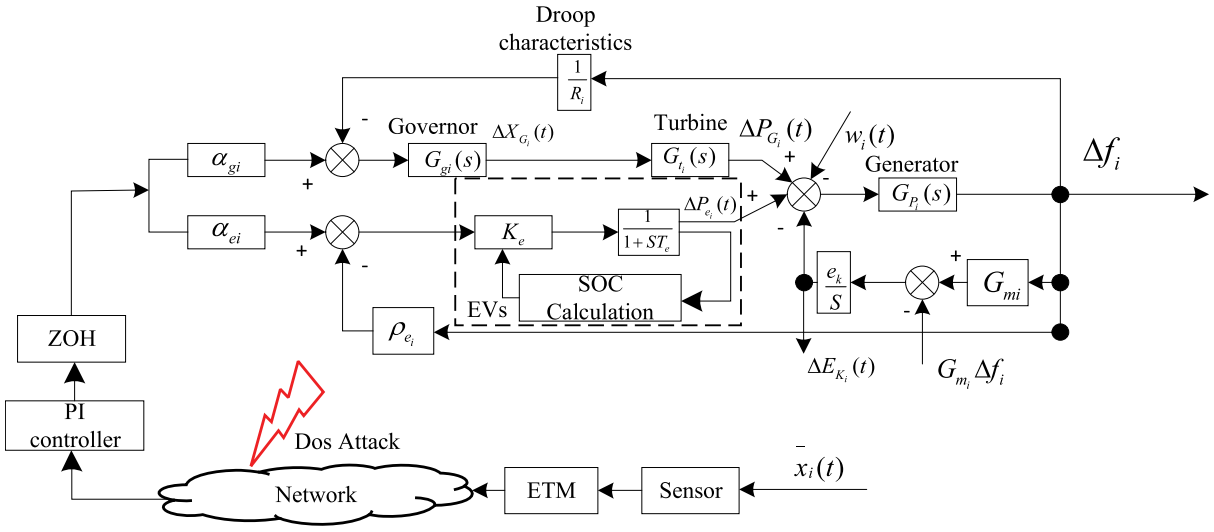

Fig. 1. Multi-area LFC CPPS model with EVs.

follows:

$$G_{gi}(s)=\frac{1}{1+sT_{gi}},\quad G_{ti}(s)=\frac{1}{1+sT_{ti}},$$
$$G_{Pi}(s)=\frac{1}{D_{pi}+sH_{pi}},\quad G_{mi}=\sum_{j=1,j\neq i}^{n}T_{ij}. \tag{1}$$

For the ith LFC CPPS, it contains Governor, Turbine, Generator, EVs and communication network, which can be seen from Fig. 1. The state–space model of the ith LFC CPPS is described as follows:

$$\begin{cases}\dot{\bar{x}}_i(t)=\bar{A}_{ii}\bar{x}_i(t)+\bar{A}_{ij}\bar{x}_j(t)+\bar{B}_i\bar{u}_i(t)+\bar{B}_{\omega_i}\bar{\omega}_i(t),\\ \bar{y}_i(t)=\bar{C}_i\bar{x}_i(t),\end{cases} \tag{2}$$

$\bar{A}_{ii}$, $\bar{A}_{ij}$, $\bar{B}_i$, $\bar{B}_{\omega_i}$, $\bar{C}_i$ are constant system matrices. The state vectors of the ith and jth system are represented by $\bar{x}_i(t)$, $\bar{x}_j(t)$ respectively. $\bar{u}_i(t)$, $\bar{\omega}_i(t)$ and $\bar{y}_i(t)$ denotes the control input, the external disturbances and the output of the ith system respectively. The system states are listed as follows:

$$\bar{x}_i(t)=col\{\Delta E_{K_i}(t),\quad \Delta X_{G_i}(t),\quad \Delta P_{G_i}(t),\quad \Delta f_i(t),\quad \Delta P_{E_i}(t)\},$$
$$\bar{\omega}_i(t)=col\{\omega_i(t),\quad 0,\quad 0,\quad 0,\quad 0\},$$
$$\bar{y}_i(t)=col\{ACE_i(t)\},\quad \bar{u}_i(t)=\Delta P_{ci}(t).$$

where $\Delta E_{K_i}(t)$, $\Delta X_{G_i}(t)$, $\Delta P_{G_i}(t)$, $\Delta f_i(t)$, $\Delta P_{E_i}(t)$, $\Delta P_{ci}(t)$ denotes tie-line power flow deviation, valve position deviation, generator mechanical output deviation, frequency deviation and power deviation of EVs, the control input respectively. The output variable $ACE_i(t)$ is the linear combination of the deviation for the frequency of area i and tie line exchange power, which is defined as $ACE_i=\Delta P_{tie,i}+\beta_i\Delta f_i$. β_i is the frequency deviation factor of area i.

Meanwhile, the differential equation models can be developed as follows based on the relationship between various modules in Fig. 1:

$$\begin{cases}\Delta\dot{E}_{Ki}(t)=e_k(G_{mi}\Delta f_i-G_{mi}\Delta f_j)\\ \Delta\dot{X}_{Gi}(t)=\frac{1}{T_{gi}}(\alpha_{gi}\Delta P_{ci}(t)-\Delta X_{Gi}(t)-\frac{1}{R_i}\Delta f_i(t))\\ \Delta\dot{P}_{Gi}(t)=\frac{1}{T_{ti}}(\Delta X_{Gi}(t)-\Delta P_{Gi}(t))\\ \Delta\dot{f}_i(t)=\frac{1}{H_{pi}}(\Delta P_{Gi}(t)+\Delta P_{ei}(t)-\Delta E_{Ki}(t)-\omega_i(t)-D_{pi}\Delta f_i(t))\\ \Delta\dot{P}_{ei}(t)=\frac{1}{T_e}(\alpha_{ei}K_e\Delta P_{ci}-\rho_{ei}K_e\Delta f_i-\Delta P_{ei}(t)).\end{cases} \tag{3}$$

Therefore, the constant system matrices in Eq. (2) can be obtained as follows:

$$\bar{A}_{ii}=\begin{bmatrix}0 & 0 & 0 & e_kG_{mi} & 0\\ 0 & -\frac{1}{T_{gi}} & 0 & -\frac{1}{R_iT_{gi}} & 0\\ 0 & \frac{1}{T_{ti}} & -\frac{1}{T_{ti}} & 0 & 0\\ -\frac{1}{H_{pi}} & 0 & \frac{1}{H_{pi}} & -\frac{D_{pi}}{H_{pi}} & \frac{1}{H_{pi}}\\ 0 & 0 & 0 & -\frac{\rho_{ei}K_e}{T_e} & -\frac{1}{T_e}\end{bmatrix},$$
$$\bar{A}_{ij}=\begin{bmatrix}0 & 0 & 0 & -e_kG_{mi} & 0\\ 0 & 0 & 0 & 0 & 0\\ 0 & 0 & 0 & 0 & 0\\ 0 & 0 & 0 & 0 & 0\\ 0 & 0 & 0 & 0 & 0\end{bmatrix},$$
$$\bar{B}_i=\begin{bmatrix}0\\ \frac{\alpha_{gi}}{T_{gi}}\\ 0\\ 0\\ \frac{\alpha_{ei}K_e}{T_e}\end{bmatrix},\quad \bar{B}_{\omega_i}=\begin{bmatrix}0 & 0 & 0 & 0 & 0\\ 0 & 0 & 0 & 0 & 0\\ 0 & 0 & 0 & 0 & 0\\ -\frac{1}{H_{pi}} & 0 & 0 & 0 & 0\\ 0 & 0 & 0 & 0 & 0\end{bmatrix},$$
$$\bar{C}_i=[1\quad 0\quad 0\quad b_i\quad 0],$$

where T_{gi}, T_{ti}, H_{Pi}, D_{Pi}, T_{ij} represents governor time constant, turbine time constant, the moment of inertia of the governor, the damping coefficient of generator and the tie-lie synchronization coefficient separately; The EVs gain, the thermal turbine, EVs participation factors and EVs droop Characteristic is represented by T_e, α_{gi}, α_{ei}, ρ_{ei} separately.

A PI controller is designed for the ith LFC CPPS as follows:

$$\bar{u}_i(t)=-K_{P_i}ACE_i(t)-K_{I_i}\int ACE_i(t), \tag{4}$$

where K_{P_i}, K_{I_i} represent control gain matrices with compatible dimensions.

Define $K_i=[K_{P_i},K_{I_i}]$, $y_i(t)=col\{\bar{y}_i(t),\int ACE_i(t)\}$ and substitute the control signal (4) into system(2), the ith LFC CPPS model can be derived as follows:

$$\begin{cases}\dot{\bar{x}}_i(t)=\bar{A}_{ii}\bar{x}_i(t)+\bar{A}_{ij}\bar{x}_j(t)-\bar{B}_iK_iy_i(t)+\bar{B}_{\omega_i}\bar{\omega}_i(t),\\ \bar{y}_i(t)=\bar{C}_i\bar{x}_i(t).\end{cases} \tag{5}$$

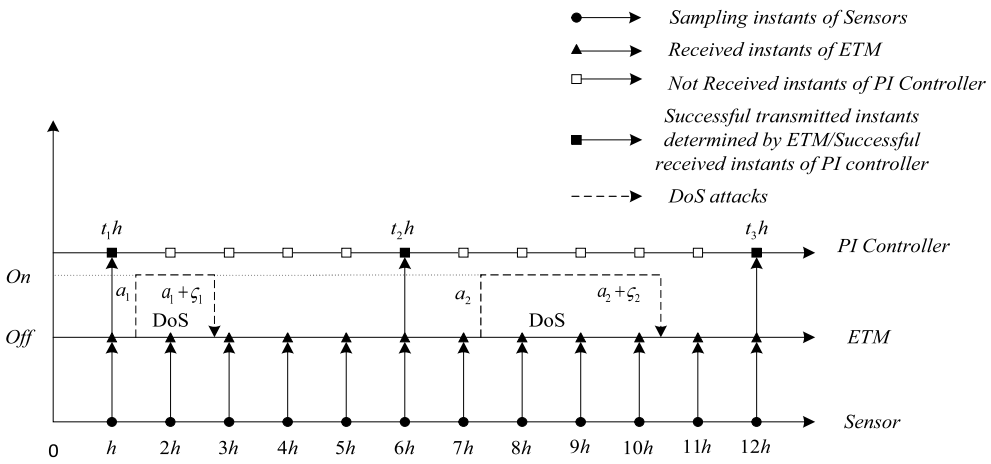

Fig. 2. Data transmission under ETM and DoS attacks.

Then define:

$$x(t) = col\{\bar{x}_1(t), \dots, \bar{x}_n(t)\}, \quad y(t) = col\{\bar{y}_1(t), \dots, \bar{y}_n(t)\},$$
$$\omega(t) = col\{\bar{\omega}_1(t), \dots, \bar{\omega}_n(t)\},$$
$$x_i(t) = col\{\bar{x}_i(t), \int ACE_i(t)\}, \tag{6}$$

the LFC model of MA-CPPS model can be established as follows:

$$\begin{cases} \dot{x}(t) = Ax(t) - BKy(t) + B_\omega\omega(t) \\ y(t) = Cx(t), \end{cases} \tag{7}$$

where A, B, C and B_ω are constant matrices, listed as follows:

$$A = [A_{ij}]_{n\times n}, \quad B = diag\{B_1, \dots, B_n\}, \quad K = diag\{K_1, \dots, K_n\},$$
$$C = diag\{C_1, \dots, C_n\}, \quad B_\omega = diag\{B_{\omega_1}, \dots B_{\omega_n}\},$$
$$A_{ii} = \begin{bmatrix} \bar{A}_{ii} & 0 \\ \bar{C}_i & 0 \end{bmatrix}, \quad A_{ij} = \begin{bmatrix} \bar{A}_{ij} & 0 \\ 0 & 0 \end{bmatrix}, \quad B_{\omega_i} = \begin{bmatrix} \bar{B}_i \\ 0 \end{bmatrix},$$
$$B_i = \begin{bmatrix} \bar{B}_{\omega i} & 0 \\ 0 & 0 \end{bmatrix}, \quad C_i = \begin{bmatrix} \bar{C}_i & 0 \\ 0 & 1 \end{bmatrix}^T,$$

2.2. Sampling-data LFC model of MA-CPPS considering AETM and DoS attacks

In practical operation of LFC MA-CPPS, sampling-data mechanism works under network environment. It can seen from Figs. 1 and 2, $\bar{x}_i(t)$ is sampled by sensor with the sampling instants sequence $\mathcal{S}_1 = \{mh\} = \{1h, 2h, 3h, \dots, mh, \dots\}$, $m \in \mathbb{R}$, where h denoting sampling interval. Then the state information $\bar{x}_i(mh)$ is transmitted to ETM. $\bar{x}_i(mh)$ is determined by ETM whether to be transmitted though network according to the triggering condition. Setting $\mathcal{S}_2 = \{t_k h\}, k \in \mathbb{R}$ indicates the successfully transmitted instants sequence determined by ETM. To simplify the analysis like Ref. [38], the network-induced delays are ignored due to their tininess compared with the transmission period of ETM in the practical operations of LFC MA-CPPS. Hence assuming the successful received instants sequence of PI controller is also expressed by $\mathcal{S}_2$. Shown in Fig. 2, it is easy to see $\mathcal{S}_2 \in \mathcal{S}_1$.

Meanwhile, some malicious attackers existing in communication networks may interfere the operation of LFC MA-CPPS and even cause its collapse. As a typical example of network attacks, DoS attack may disrupt the stability and operation of LFC MA-CPPS by blocking communication transmission with a large number of useless message, which malicious occupy the limited network bandwidth. If the network in Fig. 1 is subjected to DoS attacks, as DoS status changing from *off* to *on* in Fig. 2, some transmitting data determined by ETM are prevented from being successfully transmitted to PI controller. Define $\Theta(t)$ as the total instants set where the transmitting behaviors determined by ETM are interrupted by DoS attacks. Once the transmitting instant determined by ETM $t_k h \in \Theta(t)$, the related data $\bar{x}_i(t_k h)$ cannot be received by PI controller.

Owing to the DoS attack can disrupt the communication, the signal transmission mechanism needs to be reconsidered. Showed as Fig. 2, in the kth signal transmission period of network, define $[a_k, a_k + \varsigma_k]$ as DoS attack period, where $\varsigma_k = 0$ means no DoS attack in the kth signal transmission period. Thus the instants set that may be successfully transmitted to PI controller in the kth signal transmission period is defined as follows:

$$\mathbb{D}_k = \{d_k j = t_k h + nh | t_k h + nh \notin [a_k, a_k + \varsigma_k]\}, \tag{8}$$

where $n = 0, 1, \dots, n_{max}$, $j = 0, \dots, j_r$. From the above definition, it can be known that $t_k h + n_{max} h = t_{k+1} h$, $j_r = \frac{t_{k+1}h - t_k h - \Lambda_k h}{h}$, $d_k 0 = t_k h$. And Λ_k means the total number of sensor sampling instants including in $[a_k, a_k + \varsigma_k]$ in the kth signal transmission period. For example, seen from Fig. 2, in the first transmission period like $[t_1 h, t_2 h)$, the total number of sensor sampling instants including in $[a_1, a_1 + \varsigma_1]$ (Λ_1) equals to 1. Similarly, Λ_2 equals to 3 in the second transmission period $[t_2 h, t_3 h)$.

Remark 1. Different from those published modeling methods like Refs. [32,33], in which DoS attack behaviors are considered as periodic or following probabilistic distribution, DoS attacks are seen as nonuniform sampling process with limited interval in our work. Owing to the characteristics of stealth and energy limited, DoS attackers cannot execute frequently between the *off*/*on* status of attacks, and their duration ς_k should be bounded. Therefore, denote by $\Lambda = max\{\Lambda_k, k \in \mathbb{N}\}$ the maximum DoS caused data losses. If the DoS attack duration exceeds Λ, an attack detecting alarm may be triggered [38].

Assumption 1. For the characteristics of stealth and energy limited of DoS attacks, the count of continuous data losses caused by DoS attacks is denoted by Λ_k in the kth signal transmission period, which should be equal to or smaller than Λ. Note that Λ ia an integer.

In view of the above analyses, ETM considering DoS attack needs to be redesigned. Firstly, in the kth signal transmission period, the state error $e_{kj}(t)$ is denoted by:

$$e_{kj}(t) = \begin{cases} x(t_k h) - x(d_k 0) \\ \vdots \\ x(t_k h) - x(d_k j) \\ \vdots \\ x(t_k h) - x(d_k j_r). \end{cases} \tag{9}$$

Thus, according to the definition of $e_{kj}(t)$, the normal ETM [25] is listed as follows:

$$t_{k+1} h = \inf_{j\in\mathbb{N}} \{d_k j > t_k h \mid e_{kj}(t)^T W e_{kj}(t) \geq \kappa x^T(t_k h) W x(t_k h)\}, \tag{10}$$

where $W > 0$ is a matrix to be designed, and $\kappa > 0$ is a constant triggering parameter. Whether the sampling state will be transmitted to PI controller is determined by ETM. That is to say, the sampling state $x(d_k j)$ will be transmitted, once the triggering condition is met.

Most of the published ETMs only considered the triggering parameter as a constant or time varying, which is independent with state error $e_{kj}(t)$. In this work, the triggering parameter κ is set as a dynamic value inversely proportional to the $e_{kj}(t)$. The adaptive ETM (AETM) is proposed as following:

$$t_{k+1}h = \underset{j\in\mathbb{N}}{inf}\{d_k j > t_k h \mid e_{kj}(t)^T(t)We_{kj}(t) \geq \kappa(t)x^T(t_k h)Wx(t_k h)\}, \quad (11)$$

where

$$\kappa(t) = (\kappa_1 + \Delta\kappa_1(t)) - (\kappa_2 + \Delta\kappa_2(t))tanh(e_{kj}^T(t)e_{kj}(t) - (\kappa_3 + \Delta\kappa_3(t))). \quad (12)$$

Remark 2. Different from the existing method in Ref. [21], a novel AETM is proposed by our work, considering the random parameters fluctuations and changing dynamically of the threshold with $e_{kj}(t)$. In practical operation of LFC MA-CPPS, the system parameters will be likely interfered by external disturbances. $\Delta\kappa_1(t)$ and $\Delta\kappa_2(t)$ are random functions with range of $(0, \bar{\kappa}_1)$ and $(0, \bar{\kappa}_2)$, which represent the randomly disturbances. When $\kappa_2 = 0, \Delta\kappa_i = 0(i = 1, 2)$, the AETM reduces to general ETM as Eq. (10).

Remark 3. The hyperbolic tangent function $tanh(.)$ is monotonically increasing in its domain $(-\infty, \infty)$, with its range of $(-1, 1)$. And $\Delta\kappa_1(t)$ and $\Delta\kappa_2(t)$ are random functions with range of $(0, \bar{\kappa}_1)$ and $(0, \bar{\kappa}_2)$, which represent the randomly disturbances. As a result, $(\kappa_1 - \kappa_2 - \bar{\kappa}_2) \leq \kappa(t) \leq (\kappa_1 + \bar{\kappa}_1 + \kappa_2 + \bar{\kappa}_2)$. That is to say, the upper and lower bounds of $\kappa(t)$ is $(\kappa_1 + \bar{\kappa}_1 + \kappa_2 + \bar{\kappa}_2)$ and $(\kappa_1 - \kappa_2 - \bar{\kappa}_2)$, respectively.

Remark 4. From the definition of $\kappa(t)$, it can be seen that $\kappa(t)$ is a dynamic value inversely proportional to the $e_{kj}(t)$. At the same time, $e_{kj}(t)$ is defined as $e_{kj}(t) = x(t_k h) - x(d_k j)$. That is to say, when the system is subjected to malicious attacks or unexpected external disturbances, the system output state fluctuates more greatly, $e_{kj}^T(t)e_{kj}(t)$ is larger, $\kappa(t)$ becomes smaller. The triggering threshold defined in Eq. (11) becomes more likely met, more sampling packages could be transmitted though the network. However, when the system states are relatively stable and there is no malicious attack, $e_{kj}^T(t)e_{kj}(t)$ becomes smaller, $\kappa(t)$ is bigger, the triggering threshold becomes not easily satisfied, less packages could be transmitted. Though this mechanism, a better control performance could be obtained and relatively less packages can be transmitted throughout the runtime compared with the traditional ETM like (10), which will be showed in Section 4.

Considering the above AETM, a sampled-data state output feedback PI controller listed in (4) is relisted as follows:

$$\begin{cases} u(t) = KCx(t_k h) & t_k h \leq t < t_{k+1}h \\ T_k = t_{k+1}h - t_k h \in [T_{kmin}, T_{kmax}], \end{cases} \quad (13)$$

where $T_{kmax} = (\Lambda + 1)h + \bar{\tau}$ means the maximum transmitting interval, $T_{kmin} = h$ means the minimum transmitting interval, $\bar{\tau}$ is the allowable maximum of event triggering period when there is no DoS attack. Combining (7) and (13), the LFC model of MA-CPPS considering DoS attack is obtained for $t \in [t_k h, t_{k+1}h), k \in \mathbb{R}$ as follows:

$$\begin{cases} \dot{x}(t) = Ax(t) - BKCx(t_k h) + B_\omega\omega(t), \\ y(t) = Cx(t_k h), \quad T_k = t_{k+1}h - t_k h \in [T_{kmin}, T_{kmax}]. \end{cases} \quad (14)$$

Define $\tau(t) = t - d_k j, t \in [t_k h, t_{k+1}h)$. Thus $\dot{\tau}(t) = 1$ and $\tau(t) \in [0, \tau_m)$, where $\tau_m = T_{kmax}$.

Combining with the definition of $e_{kj}(t)$ before, the state–space model (14) can be rewritten as follows:

$$\begin{cases} \dot{x}(t) = Ax(t) - BKCx(t - \tau(t)) - BKCe_{kj}(t) + B_\omega\omega(t), \\ y(t) = C(x(t - \tau(t)) + e_{kj}(t)). \end{cases} \quad (15)$$

2.3. Control objective and basic lemma

A H_∞ performance analysis method is proposed for the LFC model of MA-CPPS under DoS attacks, and the state output controller is designed to ensure the following two states:

(1) For the maximum transmitting interval T_{kmax} with the energy-limited DoS attacks featured by Λ, the LFC model of MA-CPPS (15) is asymptotically stable with $\omega(t) = 0$.

(2) For the maximum transmitting interval T_{kmax} with the energy-limited DoS attacks featured by Λ and any nonzero $\omega(t) \in \mathfrak{L}_2[0, +\infty)$, the inequality $\|y(t)\| \leq \|\omega(t)\|_2$ holds even if the H_∞ performance index γ is small enough.

Next, Lemma 1 should be introduced before deriving the main results in the next section.

Lemma 1 ([25]). *$x(.) : [a, b] \to \mathbb{R}^n$ is a differentiable function. For any matrices $M_i(i = 1, 2, 3)$ and matrix $\mathcal{R} > 0$, the following inequality holds:*

$$-\int_a^b \dot{x}^T(s)\mathcal{R}\dot{x}(s)ds \leq (b-a)\psi_j^T\{M_1\mathcal{R}^{-1}M_1^T + \frac{1}{3}M_2\mathcal{R}^{-1}M_2^T + \frac{1}{5}M_3\mathcal{R}^{-1}M_3^T + Sym(M_1\varepsilon_1 + M_2\varepsilon_2 + M_3\varepsilon_3^j)\}\psi_j, \quad j = 1, 2. \quad (16)$$

Where

$$\psi_1 = col\left\{x(b), x(a), \int_a^b \frac{x(s)}{b-a}ds, \int_a^b\int_a^\rho \frac{x(s)}{(b-a)^2}dsd\rho\right\},$$

$$\psi_2 = col\left\{x(b), x(a), \int_a^b \frac{x(s)}{b-a}ds, \int_a^b\int_\rho^b \frac{x(s)}{(b-a)^2}dsd\rho\right\}$$

$$\varepsilon_1 = x(b) - x(a), \varepsilon_3^1 = x(b) - x(a) - \frac{6}{b-a}\int_a^b x(s)ds + \frac{6}{(b-a)^2}\int_a^b\int_a^\rho x(s)dsd\rho$$

$$\varepsilon_2 = x(b) + x(a) - \frac{2}{b-a}\int_a^b x(s)ds, \varepsilon_3^2 = x(b) - x(a) + \frac{6}{b-a}\int_a^b x(s)ds - \frac{6}{(b-a)^2}\int_a^b\int_a^\rho x(s)dsd\rho.$$

3. Main results

In this section, the H_∞ performance of LFC model for MA-CPPS (15) is firstly analyzed by Theorem 1. Then the event-triggering parameters and resilient PI controller gains can be obtained by Theorem 2. The resilient LFC system design process is presented in the end. Before that, some related variables are listed as follows:

$$\vartheta(t) = col\{x(t), \dot{x}(t), x(t - \tau(t)), x(t - \tau_M), \frac{1}{t - t_k h}\int_{t_k h}^t x(\beta)d\beta, \times\frac{1}{t_{k+1}h - t}\int_t^{t_{k+1}h} x(\beta)d\beta, \int_t^{t_{k+1}h}(t-\beta)\dot{x}(\beta)d\beta, \int_{t_k h}^t (t-\beta)\dot{x}(\beta)d\beta, e(t), \omega(t), g(t, x(t), x(t - \tau(t)))\},$$

$$\eta_1(t) = col\{x(t) - x(t_k h), \int_{t_k h}^t x(\beta)d\beta, \int_{t_k h}^t (t-\beta)\dot{x}(\beta)d\beta\},$$

$$\eta_2(t) = col\{x(t_{k+1}h) - x(t), \int_t^{t_{k+1}h} x(\beta)d\beta, \int_t^{t_{k+1}h}(t-\beta)\dot{x}(\beta)d\beta\}.$$

3.1. H_∞ Performance analysis

The following new Theorem 1 is achieved by a T_k related looped functional.

Theorem 1. *For given parameters $\bar{\tau}$, γ, Λ and a matrix $K \in \mathbb{R}^{n*2n}$, the system (15) is stable if there exist symmetric positive definite matrices $P_i \in \mathbb{R}^{4n*4n}(i = (1, 2))$, $R_i \in \mathbb{R}^{n*n}(i = (1, 2))$, $Q \in \mathbb{R}^{n*n}$, $Z \in \mathbb{R}^{n*n}$, any symmetric matrices $\mathcal{K}_i \in \mathbb{R}^{3n*3n}(i = (1, 2))$, any matrices $M_i \in \mathbb{R}^{3n*n}(i =$*

$(1,2))$, $N_i \in \mathbb{R}^{3n*n}(i=(1,2))$, $E_i \in \mathbb{R}^{n*n}(i=(1,2,3))$, $H \in \mathbb{R}^{n*n}$, $W \in \mathbb{R}^{n*n}$ *and* $\begin{bmatrix} Z & H^T \\ * & Z \end{bmatrix} > 0$, *such that the following inequalities hold:*

$$\begin{bmatrix} \Omega_{\beta_1}+T_k y_1 & Y_1 \\ * & -\Xi_1 \end{bmatrix} < 0, \quad \begin{bmatrix} \Omega_{\beta_2}+T_k y_1 & Y_1 \\ * & -\Xi_1 \end{bmatrix} < 0,$$
$$\begin{bmatrix} \Omega_{\beta_3}+T_k y_2 & Y_2 \\ * & -\Xi_2 \end{bmatrix} < 0, \quad \begin{bmatrix} \Omega_{\beta_4}+T_k y_2 & Y_2 \\ * & -\Xi_2 \end{bmatrix} < 0, \tag{17}$$

where $\beta_1,\beta_2,\beta_3,\beta_4$ *represents* $t=t_k h, T_k=T_{kmin}$; $t=t_k, T_k=T_{kmax}$; $t=t_{k+1}h, T_k=T_{kmin}$; $t=t_{k+1}h, T_k=T_{kmax}$, *the four situations respectively. And the details about other notations are listed as following:*

$$\begin{aligned}
\Omega &= sym(e_2^T(P_1+(\tau_m-\tau(t))P_2)e_1) - e_1^T(P_2-Q)e_1 - e_3^T Q e_3 + \tau_m^2 e_2^T e_2 \\
&\quad - \Pi_1^T \begin{bmatrix} Z & H^T \\ * & Z \end{bmatrix} \Pi_1 - \Pi_2^T K_1 \Pi_2 + \Pi_4^T K_2 \Pi_4 \\
&\quad + T_k sym(\Pi_6^T M_1 \Pi_8 + \Pi_6^T M_2 \Pi_9 + \Pi_7^T N_1 \Pi_{10} + \Pi_7^T N_2 \Pi_{11}), \\
y_1 &= sym(\Pi_2^T K_1 \Pi_3) + T_k e_2^T R_2 e_2, \quad y_2 = sym(\Pi_4^T K_2 \Pi_5) + T_k e_2^T R_1 e_2, \\
y_3 &= T_k \Pi_7^T (\sum_{j=1}^{2} \frac{1}{2j-1} N_j^T R_1^{-1} N_j) \Pi_7, \\
y_4 &= T_k \Pi_6^T (\sum_{j=1}^{2} \frac{1}{2j-1} M_j^T R_2^{-1} M_j) \Pi_6, \\
Y_1 &= [T_k \Pi_7^T N_1 \quad T_k \Pi_7^T N_2], \quad Y_2 = [T_k \Pi_6^T M_1 \quad T_k \Pi_6^T M_2], \\
\Xi_1 &= diag\{R_1, 3R_1\}, \quad \Xi_2 = diag\{R_2, 3R_2\}, \\
\Pi_1 &= col\{e_1-e_3, \quad e_3-e_4\}, \quad \Pi_2 = col\{e_1-e_3-e_9, \quad \alpha_1 e_5, \quad e_8\}, \\
\Pi_3 &= col\{e_2, \quad e_1, \quad e_1-e_3-e_9\}, \\
\Pi_4 &= col\{e_3-e_1, \quad \alpha_2 e_6, \quad e_7\}, \quad \Pi_5 = col\{-e_2, \quad -e_1, \quad e_3-e_1\} \\
\Pi_6 &= col\{e_1, \quad e_3+e_9, \quad e_5\} \\
\Pi_7 &= col\{e_3, \quad e_1, \quad e_6\}, \quad \Pi_8 = e_1-e_3-e_9, \quad \Pi_9 = e_1+e_3+e_9-2e_5, \\
e_{10} &= e_3-e_1, \quad e_{11} = e_1+e_3-2e_6, \\
e_i &= [0_{n\times(i-1)n} I_n 0_{n\times(11-i)n}], \quad \alpha_1 = t-t_k h, \quad \alpha_2 = t_{k+1}h - t.
\end{aligned}$$

Proof. The following LKF candidates are utilized to analysis the H_∞ performance.

$$V(t) = \sum_{i=1}^{2} V_i(t) + \sum_{j=1}^{2} \mathcal{V}_j(t), \tag{18}$$

where

$$\begin{aligned}
V_1(t) &= x^T(t)(P_1+(\tau_m-\tau(t))P_2)x(t), \\
V_2(t) &= \int_{t-\tau(t)}^{t} x^T(s) Q x(s) ds + \int_{t-\tau_m}^{t} t_m(s-t+\tau_m)\dot{x}^T(s) Z \dot{x}(s) ds, \\
\mathcal{V}_1(t) &= (t_{k+1}-t)\eta_1^T(t)\mathcal{K}_1\eta_1(t) + (t-t_k)\eta_2^T(t)\mathcal{K}_2\eta_2(t), \\
\mathcal{V}_2(t) &= -(t-t_k)T_k \int_{t}^{t_{k+1}h} \dot{x}^T(s) R_1 \dot{x}(s) ds \\
&\quad + (t_{k+1}h-t)T_k \int_{t_k h}^{t} \dot{x}^T(s) R_2 \dot{x}(s) ds.
\end{aligned}$$

Computing the derivative of $V(t)$ along the trajectories of system.

$$\begin{aligned}
\dot{V}_1(t) &= \vartheta^T(t)\{sym(e_2^T(P_1+(\tau_m-\tau(t))P_2)e_1) - e_1^T P_2 e_1\}\vartheta(t), \\
\dot{V}_2(t) &= \vartheta^T(t)\{e_1^T Q e_1 - e_3^T Q e_3 + \tau_m^2 e_2^T e_2\}\vartheta(t) - \tau_m \int_{t-\tau_m}^{t} \dot{x}^T(s) Z \dot{x}(s) ds,
\end{aligned} \tag{19}$$

$$\begin{aligned}
\dot{\mathcal{V}}_1(t) &= \vartheta^T(t)\{ - \Pi_2^T K_1 \Pi_2 + sym(\alpha_2 \Pi_2^T K_1 \Pi_3) + \Pi_4^T K_2 \Pi_4 \\
&\quad + sym(\alpha_1 \Pi_4^T K_2 \Pi_5)\}\vartheta(t), \\
\dot{\mathcal{V}}_2(t) &= -T_k \int_{t}^{t_{k+1}h} \dot{x}(s) R_1 \dot{x}(s) ds - T_k \int_{t_k h}^{t} \dot{x}(s) R_2 \dot{x}(s) ds \\
&\quad + \vartheta^T(t)\{\alpha_1 T_k e_2^T R_1 e_2 + \alpha_2 T_k e_2^T R_2 e_2\}\vartheta(t).
\end{aligned} \tag{20}$$

The reciprocally convex approach [25] is used to analyze the integral item in $\dot{V}_2(t)$ as follows:

$$\begin{aligned}
-\tau_m \int_{t-\tau_m}^{t} \dot{x}^T(s) Z \dot{x}(s) ds \le & - \begin{bmatrix} x(t)-x(t-\tau(t)) \\ x(t-\tau(t))-x(t-\tau_m) \end{bmatrix}^T \\
& \times \begin{bmatrix} Z & H^T \\ * & Z \end{bmatrix} \begin{bmatrix} x(t)-x(t-\tau(t)) \\ x(t-\tau(t))-x(t-\tau_m) \end{bmatrix},
\end{aligned} \tag{21}$$

where $\begin{bmatrix} Z & H^T \\ * & Z \end{bmatrix} > 0$.

By utilizing Lemma 1, the integral terms in $\mathcal{V}_2(t)$ can be converted into the following forms:

$$\begin{aligned}
& - T_k \int_{t_k}^{t} \dot{x}^T(s) R_2 \dot{x}(s) ds - T_k \int_{t}^{t_{k+1}} \dot{x}^T(s) R_1 \dot{x}(s) ds \\
\le & \vartheta^T(t)\{\alpha_1 T_k \Pi_6^T \sum_{j=1}^{2} \frac{1}{2j-1} M_j R_2^{-1} M_j^T \Pi_6 \\
& + \alpha_2 T_k \Pi_7^T \sum_{j=1}^{2} \frac{1}{2j-1} N_j R_1^{-1} N_j \Pi_7\}\vartheta(t) \\
& + \vartheta^T(t)\{Sym\{T_k \Pi_6^T M_1 \Pi_8 + T_k \Pi_6^T M_2 \Pi_9\} \\
& + Sym\{T_k \Pi_7^T N_1 \Pi_{10} + T_k \Pi_7^T N_2 \Pi_{11}\}\}\vartheta(t)
\end{aligned} \tag{22}$$

As well know, unknown disturbances in practical operation will bring negative effects in stability analysis of LFC MA-CPPS. The load disturbances are considered as time-varying nonlinear function with current and delayed state vectors as $B_\omega \omega(t) = g(t, x(t), x(t-\tau(t)))$, which satisfies the following norm-bounded constraints:

$$\begin{aligned}
& \|g(t,x(t),x(t-\tau(t)))\| \le \rho\|x(t)\| + \tau\|x(t-\tau(t))\|, \\
& g^T(t,x(t),x(t-\tau(t)))g(t,x(t),x(t-\tau(t))) \\
& \quad \le \rho^2 x^T(t) L^T L x(t) + \tau^2 x^T(t-h(t)) V^T V x(t-h(t)).
\end{aligned} \tag{23}$$

Where $\rho \ge 0$, $\tau \ge 0$ represent known scalars. L and V represent known constant matrices with appropriate dimensions. ρ, τ, L, V bound the magnitude of time-varying load disturbances of power system together.

According to the AETM condition (11), we can obtain the following inequality:

$$e_{kj}^T(t) C^T W C e_{kj}(t) - \kappa(t)(e_{kj}(t)+x(d_k j))^T C^T W C (e_{kj}(t)+x(d_k j)) > 0. \tag{24}$$

Noting the following equalities are true:

$$\begin{aligned}
e_2\vartheta(t) &= \{Ae_1 - BKCe_3 - BKCe_9 + B_\omega e_{10} + e_{11}\}\vartheta(t), \\
e_8\vartheta(t) &= -(t-t_k h)x(t_k h) + \int_{t_k h}^{t} x(\beta) d\beta = \{-\alpha_1(e_3+e_9)+e_5\}\vartheta(t), \\
e_7\vartheta(t) &= -(t_{k+1}h-t)x(t_{k+1}h) + \int_{t}^{t_{k+1}h} x(\beta) d\beta = \{-\alpha_2 e_3 + e_6\}\vartheta(t).
\end{aligned} \tag{25}$$

Assuming any matrix $E_i, (i=1,2,3)$ with suitable dimensions, the following zero equality constraints will be obtained:

$$\begin{aligned}
& 2\vartheta^T(t) e_2^T E_1 \{Ae_1 - BKCe_3 - BKCe_9 + B_\omega e_{10} + e_{11} - e_2\}\vartheta(t) = 0, \\
& 2\vartheta^T(t) e_8^T E_2 \{-\alpha_1(e_3+e_9)+e_5-e_8\}\vartheta(t) = 0, \\
& 2\vartheta^T(t) e_7^T E_3 \{-\alpha_2 e_3 + e_6 - e_7\}\vartheta(t) = 0.
\end{aligned} \tag{26}$$

Combining (19)–(26), the inequality can be obtained as follow:

$$\dot{V}(t) \le \vartheta^T(t)\Psi\vartheta(t) - y^T(t)y(t) + \gamma^2\omega^T(t)\omega(t), \tag{27}$$

where $\Psi = \frac{\alpha_2}{T_k}\Phi_1 + \frac{\alpha_1}{T_k}\Phi_2$, $\Phi_1 = \Omega + T_k(y_1+y_3)$, $\Phi_2 = \Omega + T_k(y_2+y_4)$, $y_i(i=1,2,3,4)$ have been defined in (17).

Noting $t = t_k h$ means $\alpha_1 = 0, \alpha_2 = T_k$, $\Psi = \Phi_1$, and $t = t_{k+1}h$ means $\alpha_2 = 0, \alpha_1 = T_k$, $\Psi = \Phi_2$. The inequalities (17) can be deduced from $\Phi_i(i=1,2) < 0$ by the Shur complement lemma and convex combination method. Thus the following inequality holds based on (17):

$$\dot{V}(t) \le -y^T(t)y(t) + \gamma^2\omega^T(t)\omega(t). \tag{28}$$

Therefore when $\omega(t)=0$, $\dot{V}(t)\le -\|y(t)\|$, the system(15) is asymptotically stable. Moreover, owing to $\dot{V}(t)$ is continuous in t, it takes integration both sides of (28) from 0 to $+\infty$. The following inequality can be achieved:

$$V(+\infty)-V(0)<\int_0^{+\infty}(-y^T(t)y(t)+\gamma^2\omega^T(t)\omega(t))dt. \tag{29}$$

For $\omega(t)\in L_2[0,+\infty)$, it is easily to known $\|y(t)\|_2\le\gamma\|\omega(t)\|$ from (29) because of the initial condition of $V(0)=0$. From the above analysis, the LFC MA-CPPS under DoS attack is asymptotically stable with an H_∞ performance.

Remark 5. Our proposed Theorem 1 can obtain less conservative result, owing to the LKFs we adopted have the following advantages:

(1) The looped-functionals $\mathcal{V}_l(t), l=1,2$ satisfy $\lim_{t\to t_{k+1}}\mathcal{V}_l(t)=\mathcal{V}_l(t_{k+1})=0$ and $\lim_{t\to t_k}\mathcal{V}_l(t)=\mathcal{V}_l(t_k)=0$. According to the looped-functional-based method [25], there is no need to consider the positiveness of $\mathcal{V}_l(t), l=1,2$ on the sampling interval, which may help to obtain less conservatism results.

(2) Different from the method in [38], two new time integrated states $\int_{t_k h}^{t}(t-\beta)\dot{x}(\beta)d\beta$ and $\int_{t}^{t_{k+1}h}(t-\beta)\dot{x}(\beta)d\beta$ are included in $\mathcal{V}_1(t)$. The addition states bring more cross terms of variables, which may reduce the conservatism of our results.

(3) A T_k-dependent looped functional $\mathcal{V}_2(t)$ is proposed. The simple Lemma 1 is used to estimate the integral terms in $\dot{\mathcal{V}}_2(t)$. Different from the method in [38], where larger conservatism inequalities without free matrices are adopted for estimating the integral terms, the introducing of free-matrices based inequalities by Lemma 1 can reduce the conservatism.

3.2. Resilient H_∞ controller design

Based on the above Theorem 1, the following Theorem 2 is provided to design PI controllers for system(15) with a guaranteed H_∞ performance and bounded DoS attack period.

Theorem 2. *For given parameters $\bar{\tau}$, γ Λ, the system (15) is stable if there exist symmetric positive definite matrices $\bar{P}_i\in\mathbb{R}^{4n*4n}(i=(1,2))$, $\bar{R}_i\in\mathbb{R}^{n*n}(i=(1,2))$, $\bar{Q}\in\mathbb{R}^{n*n}$, $\bar{Z}\in\mathbb{R}^{n*n}$, any symmetric matrices $\bar{\mathcal{K}}_i\in\mathbb{R}^{3n*3n}(i=(1,2))$, any matrices $\bar{M}_i\in\mathbb{R}^{3n*n}(i=(1,2))$, $\bar{N}_i\in\mathbb{R}^{3n*n}(i=(1,2))$, $\bar{E}_i\in\mathbb{R}^{n*n}(i=(2,3))$, $X\in\mathbb{R}^{n*n}$, $g\in\mathbb{R}^{2n*2n}$, $\mathcal{N}\in\mathbb{R}^{n*2n}$, $\bar{H}\in\mathbb{R}\in\mathbb{R}^{n*n}$, $\bar{W}\in\mathbb{R}^{n*n}$ and $\begin{bmatrix}\bar{Z} & \bar{H}^T\\ * & \bar{Z}\end{bmatrix}>0$, such that the following inequalities hold:*

$$\begin{bmatrix}\bar{\Omega}_{\beta_1}+T_k\bar{y}_1 & \bar{Y}_1\\ * & -\bar{\Xi}_1\end{bmatrix}<0,\quad \begin{bmatrix}\bar{\Omega}_{\beta_2}+T_k\bar{y}_1 & \bar{Y}_1\\ * & -\bar{\Xi}_1\end{bmatrix}<0,$$
$$\begin{bmatrix}\bar{\Omega}_{\beta_3}+T_k\bar{y}_2 & \bar{Y}_2\\ * & -\bar{\Xi}_2\end{bmatrix}<0,\quad \begin{bmatrix}\bar{\Omega}_{\beta_4}+T_k\bar{y}_2 & \bar{Y}_2\\ * & -\bar{\Xi}_2\end{bmatrix}<0, \tag{30}$$

$$\begin{bmatrix}-\ell\times I_{5n\times 5n} & (gC-CX)^T\\ * & -I_{2n\times 2n}\end{bmatrix}<0. \tag{31}$$

$$\begin{aligned}\bar{\Omega}&=sym(e_2^T(\bar{P}_1+(\tau_m-\tau(t))\bar{P}_2)e_1)-e_1^T(\bar{P}_2-\bar{Q})e_1-e_3^T\bar{Q}e_3+\tau_m^2e_2^Te_2\\&\quad-\Pi_1^T\begin{bmatrix}\bar{Z} & \bar{H}^T\\ * & \bar{Z}\end{bmatrix}\Pi_1-\Pi_2^T\bar{K}_1\Pi_2+\Pi_4^T\bar{K}_2\Pi_4\\&\quad+T_k sym(\Pi_6^T\bar{M}_1\Pi_8+\Pi_6^T\bar{M}_2\Pi_9+\Pi_7^T\bar{N}_1\Pi_{10}+\Pi_7^T\bar{N}_2\Pi_{11}),\\ \bar{y}_1&=sym(\Pi_2^T\bar{K}_1\Pi_3)+T_ke_2^T\bar{R}_2e_2,\quad \bar{y}_2=sym(\Pi_4^T\bar{K}_2\Pi_5)+T_ke_2^T\bar{R}_1e_2,\\ \bar{y}_3&=T_k\Pi_7^T(\sum_{j=1}^{2}\frac{1}{2j-1}\bar{N}_j^T\bar{R}_1^{-1}\bar{N}_j)\Pi_7,\\ \bar{y}_4&=T_k\Pi_6^T(\sum_{j=1}^{2}\frac{1}{2j-1}\bar{M}_j^TR_2^{-1}\bar{M}_j)\Pi_6,\\ \bar{Y}_1&=[T_k\Pi_7^T\bar{N}_1\quad T_k\Pi_7^T\bar{N}_2],\quad \bar{Y}_2=[T_k\Pi_6^T\bar{M}_1\quad T_k\Pi_6^T\bar{M}_2],\\ \bar{\Xi}_1&=diag\{\bar{R}_1,3\bar{R}_1\},\quad \Xi_2=diag\{\bar{R}_2,3\bar{R}_2\},\end{aligned}$$

Proof. Let $Y=E_1^{-1}$, $\mathcal{Y}_m=diag\{Y\dots Y\}_{m\times m}$, then $\bar{P}_i=\mathcal{Y}_4^TP_i\mathcal{Y}_4(i=1,2)$, $\bar{R}_i=\mathcal{Y}_1^TR_i\mathcal{Y}_1(i=1,2)$, $\bar{Q}=\mathcal{Y}_1^TQ\mathcal{Y}_1$, $\bar{Z}=\mathcal{Y}_1^TZ\mathcal{Y}_1$, $\bar{K}_i=\mathcal{Y}_3^TR_i\mathcal{Y}_3(i=1,2)$, $\bar{M}_i=\mathcal{Y}_3^TM_i\mathcal{Y}_1(i=1,2)$, $\bar{N}_i=\mathcal{Y}_3^TN_i\mathcal{Y}_1(i=1,2)$, $\bar{E}_i=\mathcal{Y}_1^TE_i\mathcal{Y}_1(i=2,3)$. Noting there is no feasible solution of the control gain matrix K, because C is a singular matrix. Inspired by the work in Ref. [39], define $KCX\triangleq\mathcal{N}C$ and $CX\triangleq gC$ with appropriate dimensions matrices $\mathcal{N}$ and g. Then we can know $(gC-CX)^T(gC-CX)-\ell I=0$ with a small enough ℓ because of $(gC-CX)^T(gC-CX)=0$, which can be converted into an optimization problem in the form of (31) by utilizing Schur complement. By pre- and post-multiplying both sides of (17) by $\mathcal{Y}_{15}^T$ and $\mathcal{Y}_{15}$ separately, the inequalities (30) can be acquired. Therefore, the PI controller gain K can be designed as:

$$K=\mathcal{N}g^{-1}. \tag{32}$$

The proof is completed. By setting T_{kmin} and T_{kmax} separately, Theorem 2 can be utilized to design PI controllers for system with an H_∞ performance index γ_{min} and a resilience DoS attack period Λ.

3.3. Resilient LFC scheme design process

The detailed design process of our proposed resilient LFC scheme can be presented as following:

S1 Modeling according to Section 2 and determining the system parameters.

S2 Controller designing. The effect of the disturbance (or the DoS attack) could be mitigated by minimizing γ (or maximizing Λ). Based on the above Theorem 2, the resilient H_∞ controller design algorithm can be presented in Fig. 3:

The Algorithm1 can be summarized by the following:

- *Step1:* Input the LFC MA-CPPS parameters, the DoS caused data losses Λ (or the H_∞ performance index γ), an accuracy coefficient γ_{ac} (or Λ_{ac}) and a search interval of H_∞ performance index $[\gamma_{min},\gamma_{max}]$ (or a search interval of DoS caused data losses $[\Lambda_{min},\Lambda_{max}]$). Denote variables $\bar{P}_i(i=(1,2))$, $\bar{R}_i(i=(1,2))$, $\bar{Q}$, $\bar{Z}$, $\bar{\mathcal{K}}_i(i=(1,2))$, $\bar{M}_i(i=(1,2))$, $\bar{N}_i(i=(1,2))$, $\bar{E}_i(i=(2,3))$, X, g, $\mathcal{N}$, $\bar{H}$, $\bar{W}$;
- *Step2:* Check if the LMIs (30)–(31) are feasible for system (15) with a tested H_∞ performance index $\gamma_{test}=(\gamma_{min}+\gamma_{max})/2$ (or with a tested DoS caused data losses $\Lambda_{test}=(\Lambda_{min}+\Lambda_{max})/2$);
- *Step3:* If the LMIs (30)–(31) are feasible, setting $\gamma_{max}=\gamma_{test}$ (or $\Lambda_{min}=\Lambda_{test}$); If inequalities (30)–(31) are unfeasible, setting $\gamma_{min}=\gamma_{test}$ (or $\Lambda_{max}=\Lambda_{test}$);
- *Step4:* Once $|\gamma_{max}-\gamma_{min}|<\gamma_{ac}$ (or $|\Lambda_{max}-\Lambda_{min}|<\Lambda_{ac}$), the minimum $\gamma_{min}=\gamma_{test}$ (or $\Lambda_{max}=\Lambda_{test}$) can be obtained, and the resilient H_∞ controller can be obtained. else go to step2.

S3 Case verification. The impact of DoS attack on our proposed AETM is studied by one-area LFC CPPS and the guaranteed H_∞ performance with the resilient DoS attack of our designed PI controller is studied by three-areas CPPS.

Remark 6. The effect of the disturbance (or the DoS attack) could be mitigated by minimizing γ (or maximizing Λ). Fixing the DoS attack index Λ, and giving an accuracy coefficient γ_{ac}, as well as a search interval of H_∞ performance index $[\gamma_{min},\gamma_{max}]$, we can find the minimum of γ and the controller gain according to Algorithm1, which means the designed controller can minimize the effect of disturbance. Meanwhile, the H_∞ performance index γ, an accuracy coefficient Λ_{ac}, and a search interval of the DoS attack index $[\Lambda_{min},\Lambda_{max}]$ are given, we can find the maximum of Λ and the controller gain according to Algorithm1, which means the designed controller can maximize the tolerance of DoS attacks for LFC system.

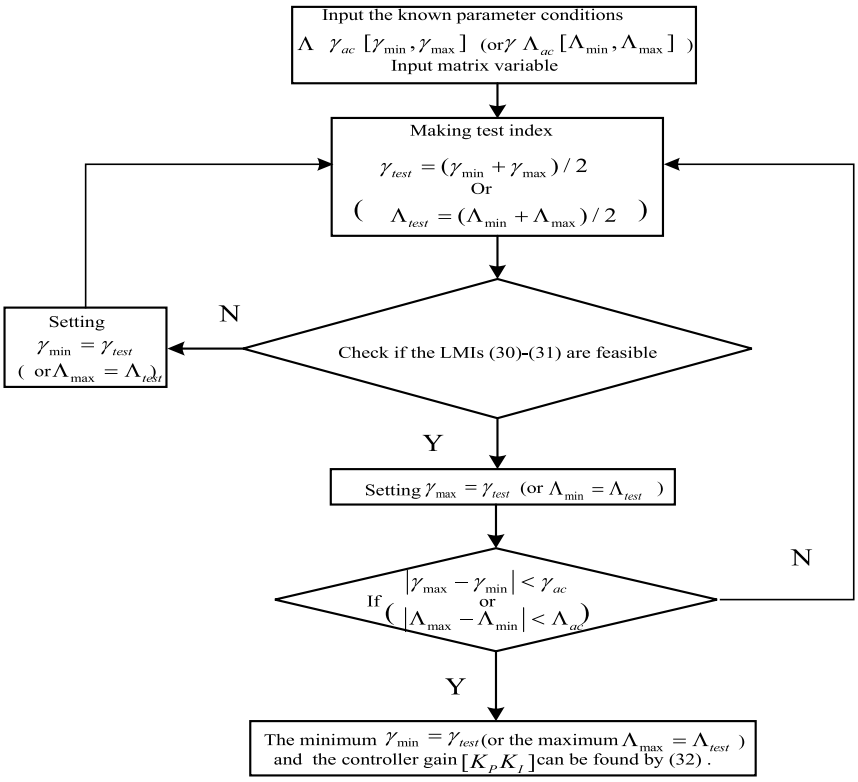

Fig. 3. The resilient H_∞ controller design Algorithm1 with given Λ and the range of γ(or given γ and the range of Λ).

Table 1
Parameters of one-area LFC system.

T_l(s)	T_g(s)	H_p(pu s)	D_p(pu/Hz)	b(pu/Hz)	R(Hz/pu)
0.3	0.08	0.1667	0.0083	0.42	2.4

4. Case studies

For verifying the effectiveness of our proposed resilient H_∞ LFC scheme based on AETM and DoS attack, two numerical examples are showed in this section. Firstly, one-area LFC CPPS [25] is presented to study the impact of DoS attacks on AETM. Secondly, three-areas LFC CPPS [38] is presented to study the resilient H_∞ control with DoS attacks.

4.1. Case study on impact of DoS attacks on AETM for CPPS

The parameters of one-area LFC CPPS given in [25] are showed in Table 1. The definition of symbols in Table 1 have been explained in Section 2. In order to study the impact of DoS attack on AETM for CPPS, the following three comparative cases (Case I, Case II, Case III) are presented. Meanwhile, setting $K_e = 1$, $T_e = 1$, $\alpha_e = 0.2$, $\alpha_g = 0.8$, $\rho_e = 0.42$, $R = 2.4$, $e_k = 2\pi$, $\omega_i(t) = 0.01$, $\bar{\tau} = 4$ and H_∞ performance index $\gamma = 7$ as Ref. [25]. And the initial state of one-area LFC CPPS is set as $x(0) = col\{0.1, 0.09, -0.14, -0.10, 0.11\}$.

Case I: No DoS attacks

If there is no DoS attack, which means $\Lambda = 0$, the output state-feedback PI controller K and the triggered matrix W in (11) are obtained by Theorem 2 as follows:

$$K = [-0.4440 \; -0.0001], \quad W = 10^8 * \begin{bmatrix} 1.0951 & 0 \\ 0 & 0.8436 \end{bmatrix}. \tag{33}$$

The state responses of system (15) with the above designed controller K are presented in Fig. 3. The release instants under the tradition ETM like (10) and our proposed AETM like (11) are depicted in Fig. 5 and Fig. 6 respectively. From Fig. 4, obviously the system states converge to zero with a good performance under our designed controller K. There are 189 data packets are transmitted when the traditional ETM is adopted, however only 60 data packets are needed to transmitted in our proposed AETM, which shows the AETM can reduce the occupation of network bandwidth in the condition of system converging to zero. Also it can be seen from Figs. 5 and 6, compared with the traditional ETM, our proposed AETM can effectively reduce average triggered intervals (ATI) by dynamically adjusting triggering parameter on the premise of ensuring the stability of the system.

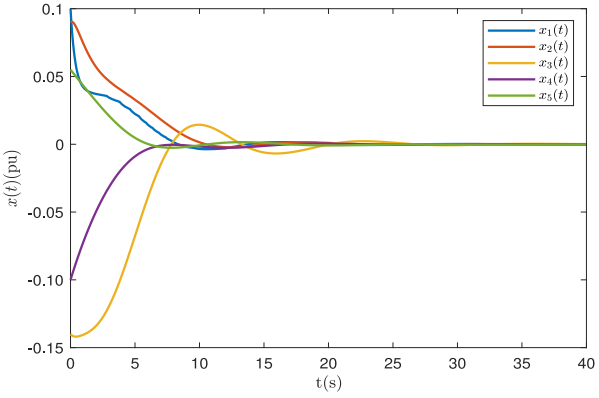

Fig. 4. State responses of LFC system with Case I.

Case II: Probabilistic DoS attacks

If there are DoS attacks imposed on communication network of system, the AETM should be adjusted. At the same time, when setting $\gamma = 7$ and $[\Lambda_{min}, \Lambda_{max}] = [0, 20]$, the maximum allowable DoS attack period is obtained as $\Lambda = 8$ by the resilient H_∞ controller design Algorithm1 presented in Fig. 3. The output state-feedback PI controller

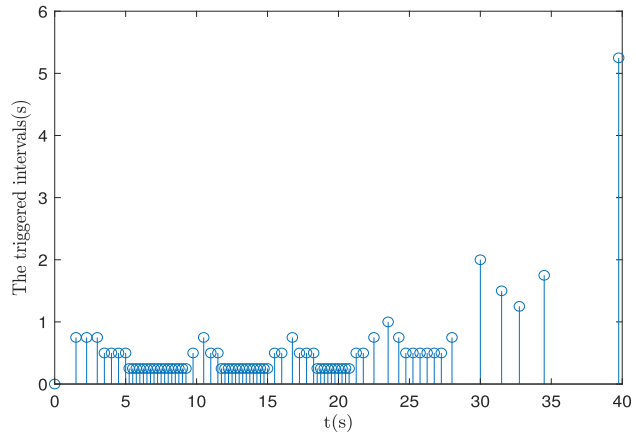

Fig. 5. Release instants under traditional ETM with Case I.

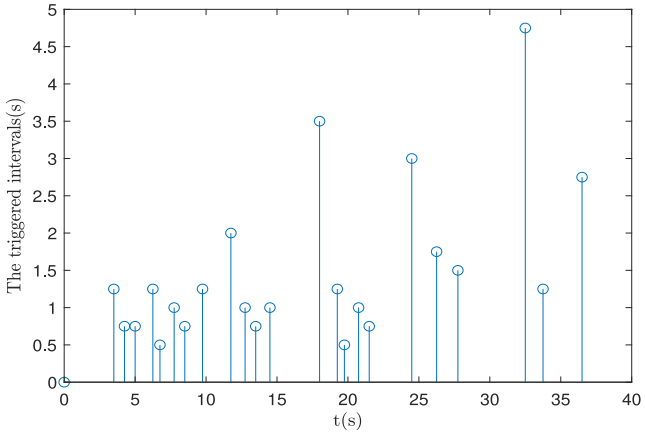

Fig. 6. Release instants under proposed AETM with Case I.

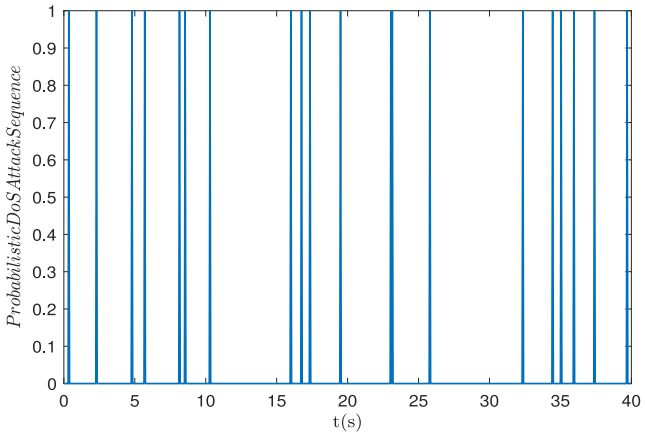

Fig. 7. Probabilistic DoS attacks with $o = 0.02$.

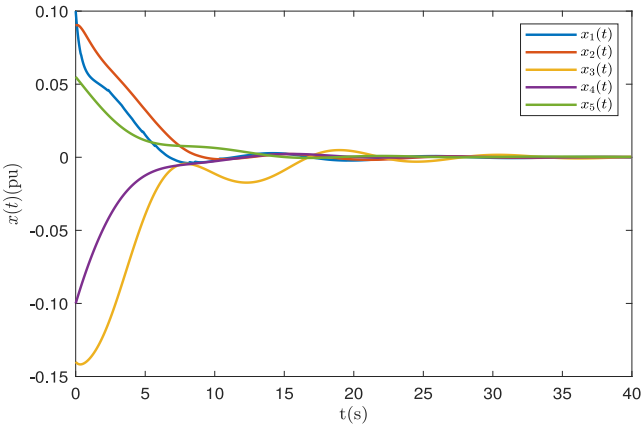

Fig. 8. State responses of LFC system with Case II.

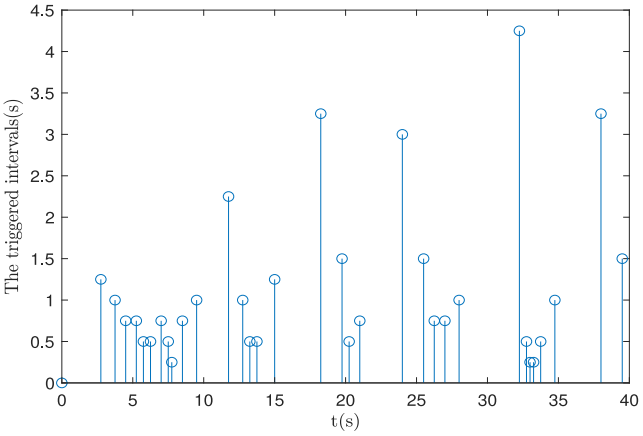

Fig. 9. Release instants under proposed AETM with Case II.

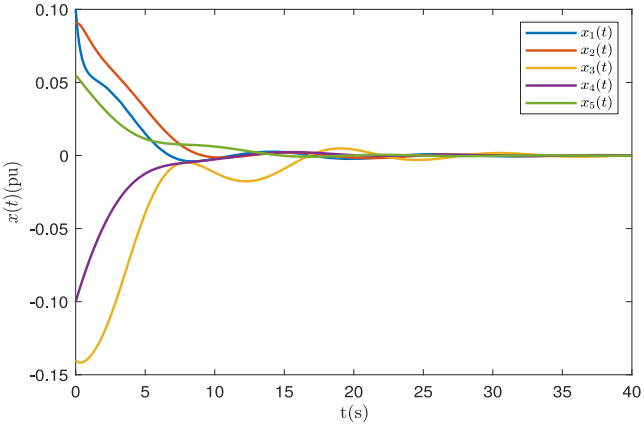

Fig. 10. State responses of LFC system with Case III.

K and the triggered matrix W are obtained as follows:

$$K = [-0.1352 - 0.0000], \quad W = 10^3 * \begin{bmatrix} 3.5652 & -0.0025 \\ -0.0024 & 0.6333 \end{bmatrix} \tag{34}$$

Suppose the probabilistic of DoS attacks obeying the Bernoulli distribution with DoS attack probability $o = 0.02$, which is presented in Fig. 7. Also, it can be seen from Fig. 8, with our designed PI controller, the state response of system (15) under the probabilistic DoS attack is asymptotic stable. Fig. 9 shows the release instants under proposed AETM with the probabilistic DoS attack. In contrast to Fig. 6, the triggered frequency is more frequent under Case II. Owing to the losses of system data caused by DoS attack making the system state changing violently, the trigger conditions are met more frequently, which has been analyzed in Remark 4.

Case III: The worst DoS attacks

Under the worst DoS attack case with $\Lambda = 8$, DoS attacks always hold until reach the upper limit of $\Lambda = 8$. Similarly, It can be seen from Fig. 10, our designed controller can still make the system asymptotic

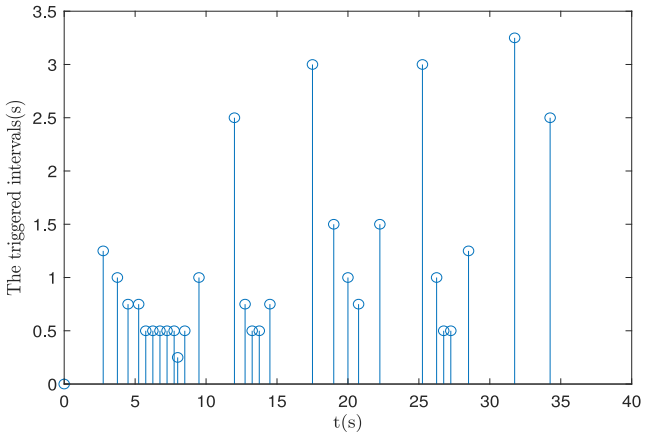

Fig. 11. Release instants under proposed AETM with Case III.

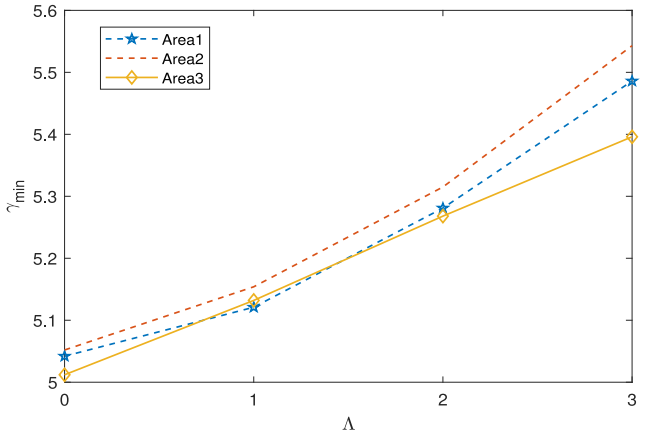

Fig. 12. The minimal γ_{min} for different DoS-limits Λ and controller for three-areas CPPS.

Table 2
Transmitting data packages under different situations.

	Case I under ETM	Case I under AETM	Case II	Case III
Data package	189	60	128	169

Table 3
The Comparison of ATI.

	[40]	[5]	[25]	Case I	Case II	Case III
ATI	0.18	1.11	1.475	1.63	1.06	0.96

stable under the worst DoS attacks. Fig. 11 shows the triggering of AETM is more frequent than Case II, owing to the system needs more control signals to reach stable state under the worst DoS attacks.

Furthermore, the transmitting data packages under the above four situations are listed in Table 2. When there is no DoS attack, our proposed AETM can greatly reduce the number of transmitting data packages, compared with the traditional ETM. And when there are DoS attacks (Case II, Case III), the packages needed to be transmitted are more than Case I, which has been analyzed in Remark 4. In addition, there are more data packages needed to transmitted in Case III than Case II, because the more serious DoS attacks in Case III need more control signals to reach the stable state than Case II. Meanwhile, the average triggered intervals(ATI) in Case I–Case III are listed in Table 3, compared with the results in [5,25,40]. Noting that the larger ATI means the better performance of reducing network bandwidth occupation. Obviously, the maximum ATI is in Case I, when there is no DoS attack in communication network as the situation in [5,25,40]. It

Table 4
Parameters of three-area LFC system.

Areas	T_i(s)	T_g(s)	H_p(pu s)	D_p(pu/Hz)	b(pu/Hz)	R(Hz/pu)
1	0.3	0.1	10	1	21	0.05
2	0.4	0.17	12	1.5	21.5	0.05
3	0.35	0.2	12	1.8	21.8	0.05
T_{ij}(pu/rad)	$T_{12} = T_{21} = 0.1986$	$T_{13} = T_{31} = 0.2148$	$T_{23} = T_{32} = 0.1830$			

Table 5
The H_∞ performance index γ_{min} under different DoS-limits Λ and controller for three-areas CPPS.

Λ	0	1	2	3
K_1	5.042	5.121	5.281	5.486
K_2	5.052	5.154	5.681	5.882
K_3	5.012	5.132	5.268	5.396

can be concluded that the proposed AETM can effectively reduce the occupation of communication network bandwidth and data computation of LFC CPPS, compared with the results in [5,25,40]. In addition, it can be observed from Table 3, the ATIs in Case II and Case III are smaller than Case I, owing to the fact of the PI controllers requiring more data from sensor to make system converging to stable when the communication channels are attacked by DoS attack, resulting in less ATIs compared with Case I. Meanwhile, as the intensification of DoS attacks, the trigger frequency increases and ATI decreases, which can be seen from the result of ATI in Case III being less than Case II in Table 3.

4.2. Case study on resilient H_∞ control with DoS attack

For further verifying the validity of our proposed method, a three-areas LFC CPPS example published in Ref. [38] is considered to study the resilient H_∞ control with DoS attack. Assume that the control structure presented in Fig. 1 is adopted by each area. The parameters of three-areas CPPS are listed in Table 4.

Under the circumstance of $T_{kmin} = 1, T_{kmax} = 8, \bar{\tau} = 4$, it can be deduced that the sampling period of sensor is $h = 1$, and the maximum DoS caused data losses $\Lambda = 3$. Meanwhile setting $\gamma_{min} = 1$ and $\gamma_{max} = 20$. Based on Algorithm1 and Theorem 2, the resilient H_∞ controller and triggered matrix W for the three-areas CPPS are designed as follows:

$$K_1 = [-0.0343 - 0.0033], \quad K_2 = [-0.0545 - 0.0083], \quad K_3 = [-0.0443 - 0.0053],$$

$$W = \begin{bmatrix} 0.1919 & -0.0231 & 0 & 0 & 0 & -0.012 \\ 0 & 225.5111 & 0 & 0 & 0 & -0.0231 \\ 0 & -0.9029 & 0.1226 & 0 & 0 & 0 \\ 0 & 0.1323 & -0.0331 & -0.0452 & -0.0431 & 0 \\ -0.0141 & -0.0532 & 0 & 0 & -0.0451 & 0 \\ 1.0960 & 1.1166 & 0 & 0 & 0 & -0.0231 \end{bmatrix} \tag{35}$$

Under the different value of Λ from 0 to 3, the obtained controllers $K_1 - K_3$ are brought into Theorem 1 to verify the minimum values of γ_{min}, which are listed in Table 5. For facilitating the observation, these results are also presented in Fig. 12. It can be seen from Fig. 12 and Table 5, when DoS-limit Λ varies from 0 to 3, the designed controllers $K_1 - K_3$ of each area can ensure the H_∞ performance index γ_{min} decreasing in a small range, which shows that the designed controllers are resilient to the energy-limited DoS attacks meanwhile guaranteeing H_∞ performance.

In the end, for the three-areas LFC CPPS with EVs, the initial states of $\Delta f_i(t)$ and $\Delta P_{iEV}(t)(i = 1, 2, 3)$ are set as $\Delta f_i(t) = 0.02$ and $\Delta P_{iEV}(t)(i = 1, 2, 3) = 0$. In the condition of designed H_∞ controllers, the frequency deviations $\Delta f_i(t)(i = 1, 2, 3)$ are showed in Fig. 13, which means frequency tends to an equilibrium point in the end. Similarly, the deviations of EVs power in three areas are depicted in Fig. 14. With the

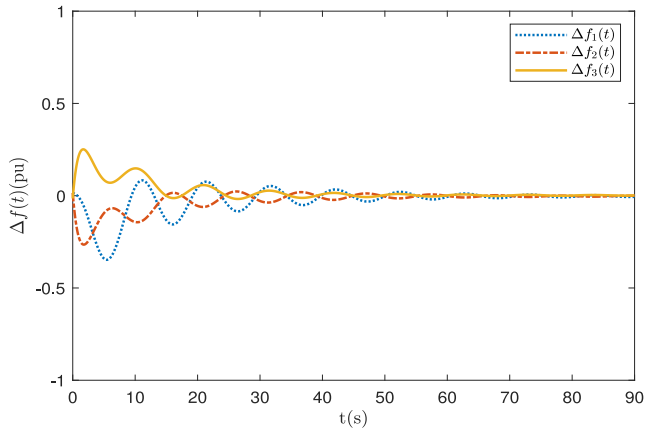

Fig. 13. The frequency deviation $\Delta f(t)$ of three-areas CPPS.

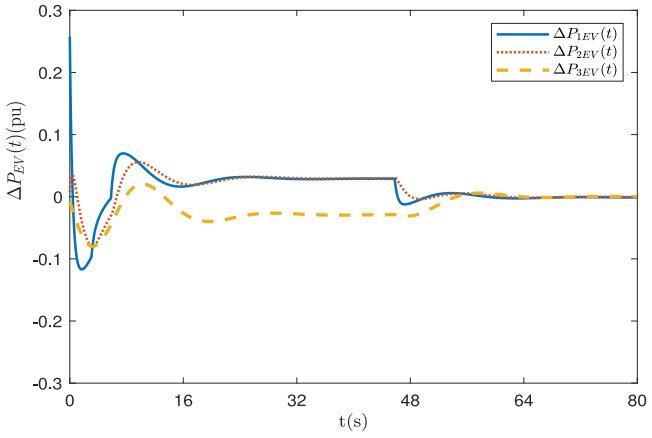

Fig. 14. The EVs power deviations of three-areas CPPS.

designed H_∞ resilient PI controllers $K_1 - K_3$, $\Delta P_{iEV}(t)(i = 1, 2, 3)$ can be brought back to zero, which also called equilibrium point. Hence the effectiveness of our designed H_∞ resilient PI controllers for LFC MA-CPPS is verified.

5. Conclusion

The event-triggered-based resilient H_∞ LFC scheme under DoS attacks for the MA-CPPS with EVs was investigated in this paper. By bounding the DoS attacks with a resilient index, which was described by maximum allowable continuous data loss counts, as well as considering the parameters disturbances and dynamic adjustment mechanism of triggered threshold in novel AETM, we constructed the sampled-data LFC model of MA-CPPS based on input-delay method with AETM and DoS attack. Additionally, we developed the H_∞ performance analysis method (Theorem 1) and H_∞ control scheme (Theorem 2) under DoS attacks based on AETM transmission interval-dependent loop functional approach, which can acquire the control gains with the guaranteed H_∞ performance and resilience index of DoS attacks. Case studies showed that our proposed AETM under DoS attack is more effective and superior, and our designed H_∞ controller can ensure the guaranteed H_∞ performance with the resilient DoS attack. Nevertheless, the security threats generally do not exist independently in actual communication network, and the network attacks exist not only in the network channel from the sensor to the control center, but also in the network channel from the control center to the generator. Therefore how to acquire the secure event-triggering scheme of multi-areas LFC CPPS in the simultaneous existence of various network attacks in double network channels, will be the focus of our future work.

References

[1] Ausnain Naveed, Şahin Sönmez, Saffet Ayasun, Impact of electric vehicle aggregator with communication time delay on stability regions and stability delay margins in load frequency control system, J. Mod. Power Syst. Clean Energy 9 (2021) 595–601.

[2] L. Jin, C.K. Zhang, Y. He, L. Jiang, M. Wu, Delay-dependent stability analysis of multi-area load frequency control with enhanced accuracy and computation efficiency, IEEE Trans. Power Syst. 34 (2019) 3687–3696.

[3] H. Bevrani, Robust Power System Frequency Control, Springer, New York, 2014.

[4] C. Peng, J. Zhang, H. Yan, Adaptive event-triggering H_∞ load frequency control for network-based power systems, IEEE Trans. Ind. Electron. 65 (2) (2018) 1685–1694.

[5] E. Tian, C. Peng, Memory-based event-triggering H_∞ load frequency control for power systems under deception attacks, IEEE Trans. Cybern. 50 (11) (2020) 4610–4618.

[6] T.N. Pham, S. Nahavandi, L.V. Hien, H. Trinh, K.P. Wong, Static output feedback frequency stabilization of time-delay power systems with coordinated electric vehicles state of charge control, IEEE Trans. Power Syst. 32 (5) (2017) 3862–3874.

[7] X. Yu, Y. Xue, Smart grids: A cyber–physical systems perspective, in: Pro.IEEE 2016, Vol. 104, No. 5, 2016, pp. 1058–1070, http://dx.doi.org/10.1109/JPROC.2015.2503119.

[8] Y.Y. Wang, R.J. Zhou, L. Gao, H/sub/spl infin//controller design for power system load frequency control, in: Proc IENCON'93. IEEE Region 10 Int Conf Computers, Communications and Automation, Vol. 5, pp. 68–71.

[9] M. Azzam, Robust automatic generation control, Energy Convers. Manage. 40 (13) (1999) 1413–1421.

[10] W. Tan, Unified tuning of PID load frequency controller for power systems via IMC, IEEE Trans. Power Syst. 25 (1) (2010) 341–350.

[11] Y. Zhang, D. Yue, S. Hu, Digital PID based load frequency control through open communication networks, in: Proc 27th Chinese Control and Decision Conf 2015, pp. 6243–6248.

[12] Y. Mi, X. Hao, Y. Liu, Y. Fu, C. Wang, P. Wang, P.C. Loh, Sliding mode load frequency control for multi-area time-delay power system with wind power integration, IET Gener. Transm. Distribution 11 (18) (2017) 4644–4653.

[13] X. Su, X. Liu, Y. Song, Event-triggered sliding-mode control for multi-area power systems, IEEE Trans. Ind. Electron. 64 (8) (2017) 6732–6741.

[14] E. Fridman, A refined input delay approach to sampled-data control, Automatica 46 (2) (2010) 421–427.

[15] A. Seuret, A novel stability analysis of linear systems under asynchronous samplings, Automatica 48 (1) (2012) 177–182.

[16] H. Zeng, K. Teo, Y. He, A new looped-functional for stability analysis of sampled-data systems, Automatica 82 (2017) 328–331.

[17] H. Luo, I.A. Hiskens, Z. Hu, Stability analysis of load frequency control systems with sampling and transmission delay, IEEE Trans. Power Syst. 35 (5) (2020) 3603–3615.

[18] X.C. Shang-Guang, Y. He, C.K. Zhang, L. Jiang, M. Wu, Sampled data based discrete and fast load frequency control for power systems with wind power, Appl. Energy 259 (2019) 114202.

[19] C. Zhao, X.Z. Liu, S.M. Zhong, K.B. Shi, D.X. Liao, Q.S. Zhong, Secure consensus of multi-agent systems with redundant signal and communication interference via distributed dynamic event-triggered control, ISA Trans. 112 (4) (2021) 89–98.

[20] D. Yue, E. Tian, Q. Han, A delay system method for designing event-triggered controllers of networked control systems, IEEE Trans. Automat. Control 58 (2) (2013) 475–481.

[21] S. Wen, X. Yu, Z. Zeng, J. Wang, Event-triggering load frequency control for multiarea power systems with communication delays, IEEE Trans. Ind. Electron. 63 (2) (2016) 1308–1317.

[22] L. Ding, Q. Han, X. Zhang, Distributed secondary control for active power sharing and frequency regulation in islanded microgrids using an event-triggered communication mechanism, IEEE Trans. Ind. Inf. 15 (7) (2019) 3910–3922.

[23] S. Hu, D. Yue, L_2-gain analysis of event-triggered networked control systems: a discontinuous lyapunov functional approach, Internat. J. Robust Nonlinear Control 23 (11) (2013) 1277–1300.

[24] L. Dong, Y. Tang, H. He, C. Sun, An event-triggered approach for load frequency control with supplementary ADP, IEEE Trans. Power Syst. 32 (1) (2017) 581–589.

[25] Q.S. Zhong, J. Yang, K.B. Shi, S.M. Zhong, Z.X. Li, M.A. Sotelo, Event-triggered H_∞ load frequency control for multi-area nonlinear power systems based on non-fragile proportional integral control strategy, IEEE Trans. Intell. Transp. Syst. (2021) 1–11.

[26] J. Liu, W. Suo, L. Zha, E. Tian, X. Xie, Security distributed state estimation for nonlinear networked systems against denial-of-service attacks, Internat. J. Robust Nonlinear Control 30 (3) (2020) 1156–1180.

[27] Y. Tang, D. Zhang, D.W.C. Ho, W. Yang, B. Wang, Event-based tracking control of mobile robot with denial-of-service attacks, IEEE Trans. Syst. Man Cybern. 50 (9) (2018) 3300–3310.
[28] M. Zhu, S. Martinez, On the performance analysis of resilient networked control systems under replay attacks, IEEE Trans. Automat. Control 59 (3) (2014) 804–808.
[29] D. Ye, T.Y. Zhang, Summation detector for false data-injection attack in cyber–physical systems, IEEE Trans. Cybern. 50 (6) (2019) 2338–2345.
[30] D. Ding, Z. Wang, Q.L. Han, G. Wei, Security control for discrete-time stochastic nonlinear systems subject to deception attacks, IEEE Trans. Syst. Man Cybern. 48 (5) (2018) 779–789.
[31] Z. Gu, X. Zhou, T. Zhang, F. Yang, M. Shen, Event-triggered filter design for nonlinear cyber–physical systems subject to deception attacks, ISA Trans. 104 (2020) 130–137.
[32] B. Niemoczynski, S. Biswas, J. Kollmer, Stability of discrete-time networked control sysyems under denial of service attacks, in: Proc Resilience Week 2016, pp. 119–124.
[33] G.K. Befekadu, V. Gupta, P.J. Antsaklis, Risk-sensitive control under Markov modulated denial-of-service(DoS) attack strategies, IEEE Trans. Automat. Control 60 (12) (2015) 3299–3304.
[34] C.D. Persis, P. Tesi, Input-to-state stabilizing control under denial-of-service, IEEE Trans. Automat. Control 60 (11) (2015) 2930–2944.
[35] X. Zhang, Q. Han, X. Ge, L. Ding, Resilient control design based on a sampled-data model for a class of networked control systems under denial-of-service attacks, IEEE Trans. Cybern. 50 (8) (2020) 3616–3626.
[36] C. Peng, J.C. Li, M.R. Fei, Resilient event-triggering H_∞ load frequency control for multi-area power systems with energy-limited DoS attacks, IEEE Trans. Power Syst. 32 (5) (2017) 4110–4118.
[37] J. Liu, Y. Gu, L. Zha, Y. Liu, J. Cao, Event-triggered H_∞ load frequency control for multiarea power systems under hybird cyber attacks, IEEE Trans. Syst. Man Cybern. 49 (8) (2019) 1665–1678.
[38] X. Zhao, S.L. Zou, Z.J. Ma, Decentralized resilient H_∞ load frequency control for cyber-physical power systems under DoS attacks, IEEE/CAA J. Autom. Sin. 8 (11) (2021) 1737–1751.
[39] C. Peng, J. Zhang, Delay-distribution-dependent load frequency control of power systems with probabilistic inteval delays, IEEE Trans. Power Syst. 31 (4) (2016) 3309–3317.
[40] H. Zhang, J. Yang, C. Su, T-S fuzzy-model-based robust H_∞ design for networked control systems with uncertainties, IEEE Trans. Ind. Inf. 3 (4) (2007) 289–301.